Mechanical Technology and Engineering Insights

www.mtei.reapress.com

Mech. Technol. Eng. Insights. Vol. 1, No. 2 (2024) 93–103.

Paper Type: Original Article

Numerical Study on the Influence of Internal Corrosion on Flow Characteristics and Pressure Drop in Water Transmission Pipes

Nayer Ali Dorostan[1,*], Mehrdad Javadi[2]

[1] Department of Energy Conversion Group, Dezful Branch, Islamic Azad University, Dezful, Iran; ali.dorostan@yahoo.com.
[2] Department of Mechatronics, South Tehran Branch, Islamic Azad University, Tehran, Iran; Javadi@azad.ac.ir.

Citation:

Received: 16 May 2024 *Revised: 26 July 2024* *Accepted: 5 September 2024*	Dorostan, N. A., & Javadi, M. (2024). Numerical study on the influence of internal corrosion on flow characteristics and pressure drop in water transmission pipes. *Mechanical Technology and Engineering Insights, 1*(2), 93-103.

Abstract

The impact of internal corrosion and rust formation in water transmission pipes is very important for hydraulic properties, flow structure, and energy losses. The current work analyzes streamlines, velocity distribution, vortex generation, and pressure coefficient changes as functions of varying degrees of internal corrosion in water transmission pipes using Computational Fluid Dynamics (CFD). CFD simulations were performed for different corrosion cases characterized by varying levels of area reduction. The Reynolds-Averaged Navier–Stokes (RANS) equations were solved in ANSYS Fluent using the finite volume method, and the Renormalization Group (RNG) k-ε turbulence model was used to account for turbulence and separated flow phenomena. Structured quadrilateral grid generation was performed in Gambit, and local grid refinement near walls and contraction areas was applied to enhance the accuracy of CFD computations. Good agreement between the CFD results and the experimental data of Eaton and Johnson on turbulent flow through a sudden expansion was obtained. From the findings, it is clear that an increase in corrosion intensity accelerates fluid flow in regions of constriction, creating high velocity and negative pressure gradients in downstream areas following the corroded parts. In addition, high levels of corrosion lead to flow separation, vortex formation, and extensive recirculation, resulting in greater hydraulic losses and pressure drop in the pipe system. From the pressure coefficient distribution plot, it is clear that severe corrosion leads to higher pressure drops in the pipe due to increased turbulence and energy losses.

Keywords: Internal corrosion, Computational fluid dynamics, Turbulent flow, Pressure drop, Water transmission pipe.

1 | Introduction

Corrosion is a major issue in the fluid transport industry, affecting not only transportation efficiency but also leading to significant equipment repair costs. Besides, corrosion alters the flow hydrodynamics, reduces the fluid transfer rate, increases the pressure drop, and increases operating costs. For example, in many water

Corresponding Author: ali.dorostan@yahoo.com
https://doi.org/10.48313/mtei.v1i2.50

supply systems, rusting and internal scale formation reduce the actual cross-sectional area of the flow and affect the flow dynamics, velocity, wall shear stress, and pressure distribution. Moreover, this problem alters the water's color, smell, and taste, causing significant problems for customers.

As a rule, corrosion is an electrochemical process in which a metal reacts with its surrounding medium. When such a reaction occurs, anodic and cathodic areas form, and, in combination with the electrolyte, oxidation and reduction occur, resulting in the formation of metal oxides and corrosion. Gradually, the roughness of the pipe wall increases, the cross-sectional area decreases, and pressure drop occurs. In turbulent flow, roughness and corrosion may lead to vortices and flow separation, increasing wall shear stress and intensifying corrosion and erosion.

Many recent studies have examined flow behavior in rough and corroded pipes. Among the early pioneers who did research on the effects of surface roughness on flow behaviors and modeled rough surfaces was Perry et al. [1]. Later, Silberman [2], [3] indicated that the internal geometry of a pipe directly affects the friction factor and flow behavior.

Due to advances in computational techniques and Computational Fluid Dynamics (CFD), flow behavior in complex geometries can now be analyzed in greater detail. For example, Chen et al. [4] conducted an experimental study on the effects of surface roughness on drag force. Djenidi et al. [5] investigated the vortex behavior generated by rough surfaces. Morales et al. [6] also compared rough and smooth surfaces and found that increased roughness increases the friction factor and pressure drop.

In recent times, much attention has been paid to the use of CFD in studying corrosion and turbulent flow in pipelines. Hu and Cheng [7] applied CFD to simulate the corrosion of a pipeline in a two-phase oil-water flow containing CO_2 and found that wall shear stress and flow structure have direct effects on corrosion. Li et al. [8] conducted a study using numerical modeling and electrochemical methods to analyze the effect of flow velocity on pipeline corrosion and concluded that higher flow velocity increases mass transfer and corrosion. Pouraria et al. [9] researched the wetting properties of the inner surfaces of oil pipelines. They noted that changes in the inner surface geometry of the pipeline affect the flow pattern, leading to localized corrosion.

Kahyarian et al. [10] reviewed the role of flow turbulence, mass transfer, and roughness on CO_2 corrosion in transmission lines. Barker et al. [11] experimentally and numerically analyzed the effect of sudden-expansion geometries on corrosion and observed that regions with flow separation and vortices exhibited higher corrosion rates. Wang et al. [12] applied CFD to study corrosion and erosion in gas-liquid pipelines and found that higher shear stress and flow instability lead to localized corrosion. Moreover, Zeng et al. [13] noted that reductions in cross-sectional area and increases in fluid velocity in constricted sections promote flow. Additionally, Thorat et al. [14] reported that the Renormalization Group (RNG) k-ε turbulence model provides high precision in predicting the flow field and corrosion rate in pipelines.

Several recent studies have examined hybrid methods and advanced models for corrosion prediction. Yang et al. [15] proposed a model that combined physics-based and active learning approaches to predict CO_2 and O_2 corrosion in pipelines via CFD and found that this approach accelerated analysis by 10^6 times. In another study, Cruz et al. [16] applied the attached eddy theory to explore the turbulent friction factor in pipes having rough walls. Wang et al. [17] studied the impact of water flow velocity on the corrosion efficiency of steel elbow pipe sections. They found that although increased flow velocity increases corrosion, its effect decreases at higher flow velocities.

Also, Obaseki et al. [18] developed a multiphase flow simulation model to predict corrosion rates in oil and gas pipelines, accounting for erosion and chloride content, with an accuracy of about 85%. Considering the significance of the topic under discussion, the present research aims to examine the influence of increased internal rusting in water pipe systems on streamline, flow velocity, and pressure coefficient via numerical simulation in Fluent. In this context, various geometries with varying internal rusting are considered, and the

impact of corrosion-induced reduction in cross-section on flow patterns, pressure variations, vortex generation, and velocity alterations is analyzed. The primary aim of the current study is to investigate the hydrodynamic behavior of flow inside corroded pipes.

2 | Governing Equations

In general, the Navier-Stokes equations govern the flow of fluids and can be used to simulate both laminar and turbulent flow regimes. However, when one tries to solve the equations directly for turbulent flow, one must use very fine meshing at all temporal and spatial scales, which makes the problem computationally expensive. Because of that, in engineering applications, averaged techniques such as RANS and LES simulations are used.

In this study, the RANS approach is employed to simulate turbulent flow. In this technique, each instantaneous variable is split into a mean and a fluctuating component. For instance, for the velocity component:

$$u_i = \bar{u}_i + u_i', \tag{1}$$

where u_i is the time-averaged velocity and u_i' is its fluctuating component. Similarly, for pressure and other scalar quantities we can write:

$$\varphi = \bar{\varphi} + \varphi', \tag{2}$$

where ϕ is an arbitrary scalar quantity, ϕ its mean value, and ϕ' its fluctuating part. By substituting the above relations into the Navier–Stokes equations and applying time averaging, the governing RANS equations are obtained as follows.

2.1 | Continuity Equation

$$\frac{\partial}{\partial x_i}(\rho u_i) = 0 \tag{3}$$

2.2 | Reynolds-Averaged Navier–Stokes Momentum Equations

$$\frac{\partial}{\partial x_i}(\rho u_i u_j) = -\frac{\partial \rho}{\partial x_j} + \frac{\partial}{\partial x_j}\left[\mu\left(\frac{\partial u_i}{\partial x_i} + \frac{\partial u_j}{\partial x_j}\right) - \frac{2}{3}\delta_{ij}\frac{\partial u_k}{\partial x_k}\right] + \frac{\partial}{\partial x_j}(-\rho u_i' u_j'). \tag{4}$$

In these equations, the last term is known as the Reynolds stresses, which arise from turbulence effects and cause the system of equations to be unclosed.

2.3 | Energy Equation

$$\frac{\partial}{\partial x_i}\left(\rho u_i\left(h + \frac{1}{2}u_j u_j\right)\right) = \frac{\partial}{\partial x_j}\left[K_{eff}\left(\frac{\partial T}{\partial x_j}\right) + u_i(\tau_{i,j})_{eff}\right], \tag{5}$$

Where

$$K_{eff} = K + \frac{C_p \mu_t}{Pr_t}. \tag{6}$$

2.4 | Modeling of Reynolds Stresses (Boussinesq Hypothesis)

To close the system of equations, the Boussinesq hypothesis is used, which relates the Reynolds stresses to the mean velocity gradient:

$$-\overline{\rho u_i' u'_j} = \mu_t \left(\frac{\partial u_i}{\partial x_j} + \frac{\partial u_j}{\partial x_i}\right) - \frac{2}{3}\left(\rho k + \mu_t \frac{\partial u_k}{\partial x_k}\right)\delta_{ij}, \quad (7)$$

where:

$$(\tau_{ij})_{eff} = \mu_{eff}\left(\frac{\partial u_j}{\partial x_i} + \frac{\partial u_i}{\partial x_j}\right) - \frac{2}{3}\mu_{eff}\frac{\partial u_k}{\partial x_k}\delta_{ij}, \quad (8)$$

$$\mu_t = \rho C_\mu \frac{k^2}{\varepsilon} \quad (9)$$

2.5 | Renormalization Group k–ε Turbulence Model

In this research, the two-equation RNG k–ε model is used to close the equations. This model includes two transport equations: one for turbulent kinetic energy kk and one for its dissipation rate ε.

2.6 | Turbulent Kinetic Energy Equation

$$\frac{\partial}{\partial x_i}(\rho k u_i) = \frac{\partial}{\partial x_j}\left[\alpha_k \mu_{eff}\frac{\partial k}{\partial x_j}\right] + 2\mu_t E_{ij}.E_{ij} - \rho\varepsilon - Y_M \quad (10)$$

2.7 | Turbulent Dissipation Rate Equation

$$\frac{\partial}{\partial x_i}(\rho \varepsilon u_i) = \frac{\partial}{\partial x_j}\left[\alpha_\varepsilon \mu_{eff}\frac{\partial \varepsilon}{\partial x_j}\right] + C^*_{1\varepsilon}\frac{\varepsilon}{k}2\mu_t E_{ij}.E_{ij} - C_{2\varepsilon}\rho\frac{\varepsilon^2}{k} - R_\varepsilon \quad (11)$$

2.8 | Effective Viscosity

$$\mu_{eff} = \mu + \mu_t. \quad (12)$$

2.9 | Renormalization Group k–ε Model Relations and Coefficients

$$C^*_{1\varepsilon} = C_{1\varepsilon} - \frac{\eta(1-\eta/\eta_0)}{1+\beta\eta^3}. \quad (13)$$

$$\eta = (2E_{ij}.E_{ij})^{1/2}\frac{k}{\varepsilon}. \quad (14)$$

$$E_{ij} = \left(\frac{\partial U_i}{\partial x_j} + \frac{\partial U_j}{\partial x_i}\right). \quad (15)$$

$$Y_M = 2\rho\varepsilon M_t^2, M_t = \sqrt{\frac{k}{\gamma RT}}. \quad (16)$$

$$R_\varepsilon = \frac{C_\mu \rho \eta^3 (1-\eta/\eta_0)}{1+\beta\eta^3}\frac{\varepsilon^2}{k}. \quad (17)$$

$$\eta_0 = 4.377, \beta = 0.012. \quad \textbf{(18)}$$

$$C_\mu = 0.0845, \alpha_k = \alpha_\varepsilon = 1.39, C_{1\varepsilon} = 1.42, C_{2\varepsilon} = 1.68, Pr_t = 0.85. \quad \textbf{(19)}$$

3 | Numerical Method

In the current study, the governing equations are solved numerically using ANSYS Fluent. Firstly, the meshing process was carried out in Gambit using a structured quadrilateral mesh. This type of mesh was chosen because it provides greater accuracy in predicting the velocity and pressure gradient in internal turbulent flow fields. Grid independence was ensured by varying mesh density and observing that finer meshes did not significantly change the outcome. Hence, grid independence is achieved. In the current simulation, a velocity inlet boundary condition is assigned at the inlet, a pressure outlet boundary condition at the outlet, and a no-slip wall boundary condition on the channel walls. The inlet velocity of water was chosen to be 1.5 m/s, and the flow was assumed to be incompressible, turbulent, and steady state. The RNG k–ε turbulence model was used for capturing the turbulence effects. *Fig. 1* shows the computational domain and the adopted meshing scheme for the numerical simulation of flow in channels with various contraction geometries. A structured quadrilateral grid was used for all simulations to enhance solution accuracy and stability. *Fig. 1a* depicts a simple channel with uniform cross-sectional dimensions, while *Figs. 1b-1f* display various contraction geometries with increasing contraction ratios. As the degree of contraction increases, the flow path narrows, leading to higher velocity gradients at the center. Furthermore, mesh refinement was performed around the walls and the contraction zones.

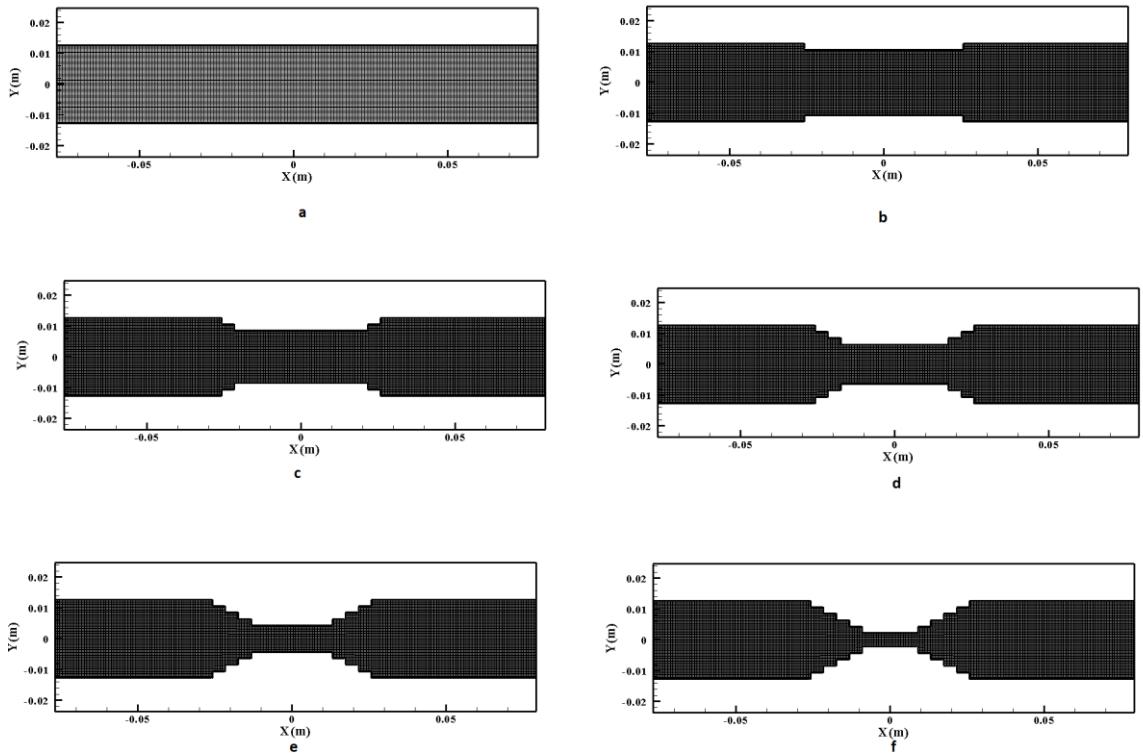

Fig. 1. Computational mesh.

4 | Result and Discussion

To validate the current numerical model, the popular example of a sudden expansion by Thangam and Speziale [19] is considered here, as it is similar to the current study. In this case, turbulent incompressible flow

(water) in a sudden expansion is analyzed, as shown schematically in the figure below. The Reynolds number, which is computed using the mean velocity at the inlet and the outlet height, is 132,000, and the expansion ratio (step height/outlet height) is 3. A fully developed velocity profile is prescribed at the inlet using a velocity inlet boundary condition, whereas a pressure outlet condition is prescribed at the outlet. Past studies concluded that the RNG k-ε turbulence model is suitable for predicting separated and recirculating flows.

Fig. 3 illustrates the dimensionless velocity distribution along the streamwise direction (u/U_0) computed by applying different turbulence models compared to the experimental data measured by Thangam and Speziale [19]. It can be seen that all turbulence models capture the flow trend satisfactorily; however, the RNG k−ε model provides the best results compared to the experimental data, especially in the recirculation and reattachment zones. Some discrepancies are found at the wall boundary and in regions of flow separation. In conclusion, the comparison demonstrates the numerical approach's ability to simulate the turbulent flow downstream of the sudden expansion.

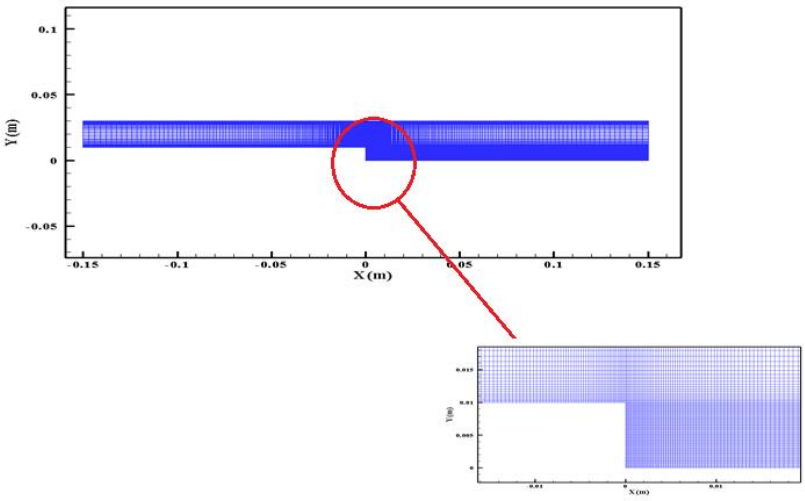

Fig. 2. Computational mesh for validate the current numerical model.

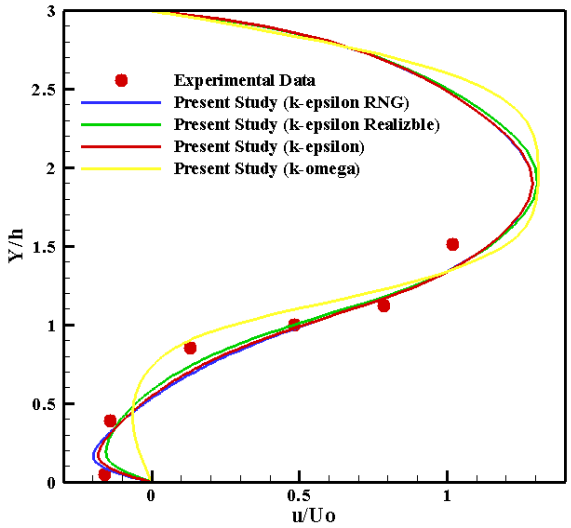

Fig. 3. Velocity distribution along (u/U_0) computed by applying different turbulence models compared to the experimental data.

Fig. 4 shows the velocity magnitude contour and streamlines of the turbulent flow in a channel with partial blockage. The constriction of the flow area leads to significant changes in the flow dynamics due to the

reduced area. According to the continuity principle, the fluid velocity increases as it flows through the constricted channel, resulting in a higher velocity magnitude at the upper part of the channel. The high-velocity region is observed on the top side of the channel due to the blockage effect.

On the other hand, a low-velocity region forms at the lower wall downstream of the blockage. Such an observation indicates a pressure gradient and flow separation that cause reverse flow in the channel due to the abrupt downstream expansion. From the streamline pattern, it can be observed that the adverse pressure gradient drives the formation of a large recirculating flow and vortices. In addition, as the area narrows, the streamlines tend to converge further, indicating an increase in shear stress and turbulence. The presence of the recirculation region demonstrates that the reduction in pipe diameter due to corrosion can significantly affect the pressure distribution and hydraulic losses. The above can be attributed to the results of previous research on turbulent separation flows and expansions. As a result, corrosion not only increases the fluid velocity within the water transmission pipe but also causes pressure loss and vortex formation.

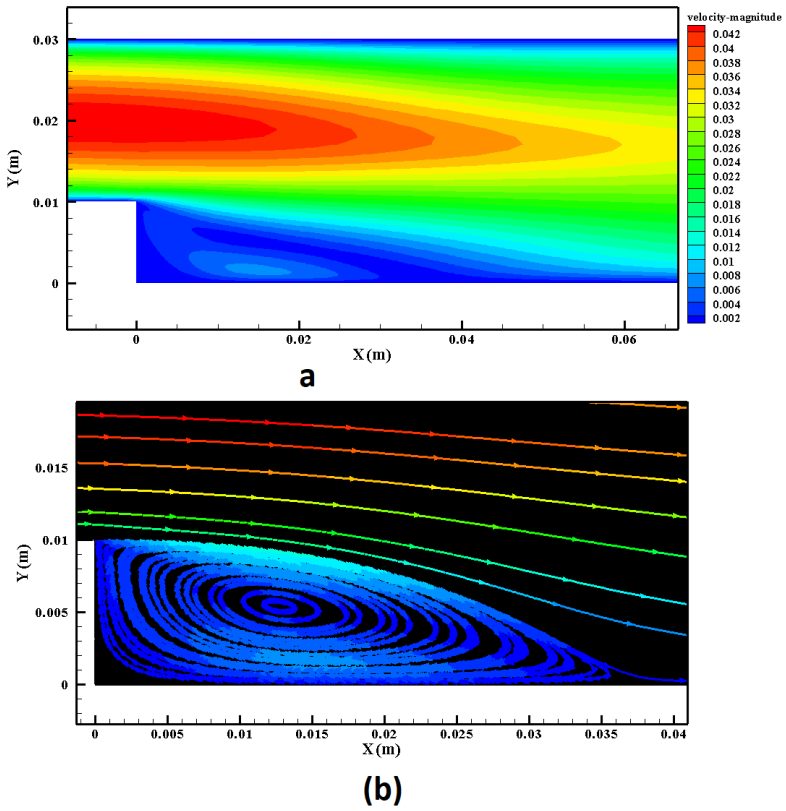

Fig. 4. Contours of velocity magnitude and streamline pattern in the corroded water transmission pipe.

Fig. 5 shows the velocity contours and streamline pattern associated with various levels of corrosion intensity in the water pipe. The constriction due to the accumulation of rust gradually decreases the available flow area from Case (a) to Case (e), resulting in significant changes to the flow dynamics.

In Case (a) of *Fig. 6*, where the pipe surface is assumed to be smooth with no corrosion effects, the flow is characterized by straight streamlines that are symmetric and stable along the length of the channel. It represents a fully developed turbulent flow with no disturbances.

With the reduction in the cross-section of the pipe in Case (b) of *Fig. 6*, a localized increase in flow speed in the reduced region is noticeable. The streamlines converge in the constricted region, while the flow structure remains quite stable compared with the smooth-pipe case. As seen in *Fig. 6c*, with further growth in corrosion strength, the level of velocity acceleration increases sharply. Moreover, a higher adverse pressure gradient forms downstream of the constriction, initiating the initial stage of flow separation near the pipe surface.

Besides, there appears to be an increased streamline curvature caused by higher turbulence activity and momentum exchange.

Fig. 6d shows that a sharp contraction of the pipe cross-section causes flow separation downstream of the corroded part. The development of large-scale vortices near the upper and lower wall surfaces occurs after the region of expansion. This occurs because of the core's deceleration and the inability to overcome the adverse pressure gradient in near-wall flow. The last case, shown in *Fig. 6e* and corresponding to the highest corrosion rate, leads to extremely disturbed flow-field behavior. The speed within the narrow throat is at its peak, and two symmetric recirculation bubbles appear behind the constriction. At the same time, the length and strength of the separation region increase significantly. Thus, it can be concluded that internal corrosion destabilizes the flow field, increases pressure losses, and generates vortices in water conveyance pipelines.

In general, the findings clearly show that increased rust buildup and decreased hydraulic diameter result in significant changes in velocity and streamline distributions, as well as in flow separation behavior. Such alterations may lead to poor hydraulic characteristics and higher energy costs for transporting fluid through such pipelines.

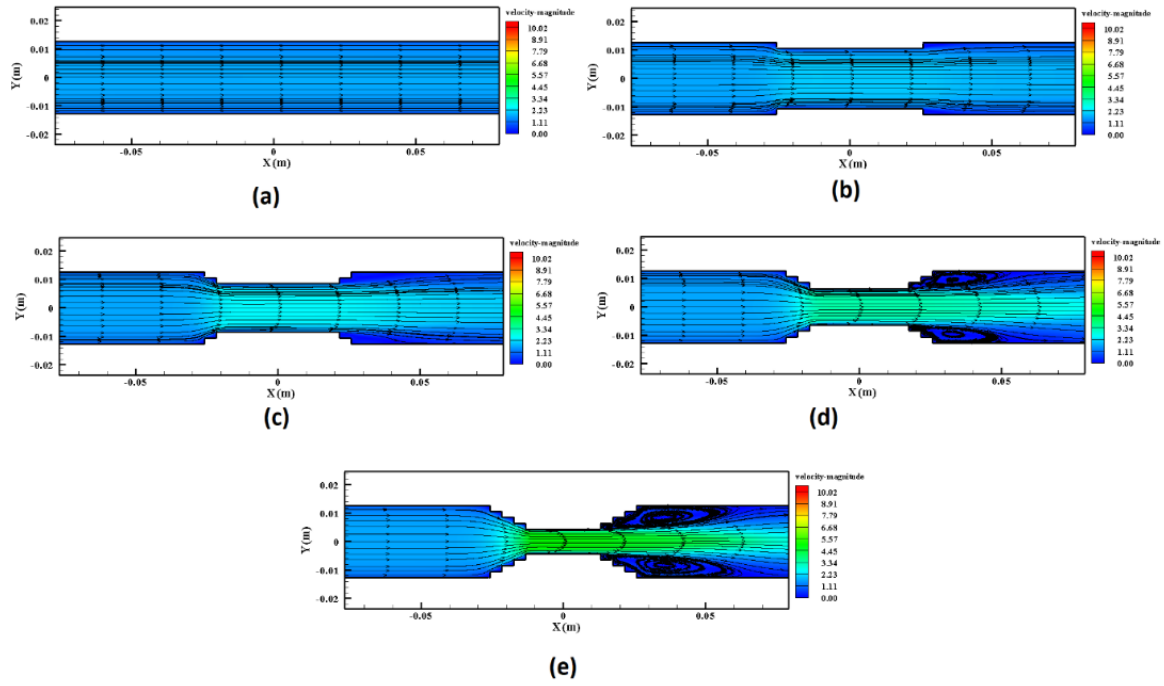

Fig. 5. Contours and streamlines for different corrosion states of internal wall surfaces and reductions in cross-sections; a) no corrosion, b) small amount of corrosion, c) moderate level of corrosion, d) high level of corrosion, and e) very high level of corrosion with developed zones of downstream recirculation.

Fig. 6 shows the variation in the pressure coefficient on the pipe surface for various internal corrosion levels. The figure shows that an increase in internal corrosion and a decrease in the effective cross-sectional area result in a dramatic reduction in the pressure within the pipe. For the smooth pipe, the pressure coefficient remains nearly constant, indicating stable fluid flow.For the smooth pipe, the pressure coefficient remains nearly constant, indicating stable fluid flow. As internal corrosion worsens, a rapid pressure reduction occurs, attributed to the adverse pressure gradient caused by the accelerated flow through the pipe section.

Beyond the section of internal corrosion, there is a slight recovery in pressure; however, pressure does not reach the initial level due to energy losses and vortex generation. Overall, the worst corrosion condition results in the highest pressure loss.

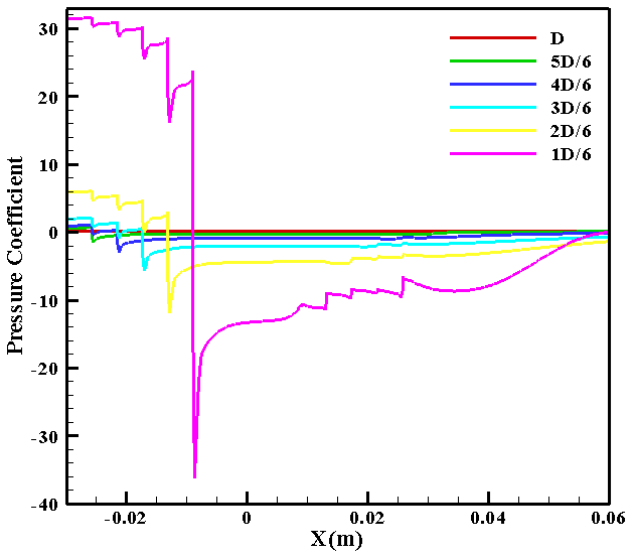

Fig. 6. Distribution of pressure coefficients along the pipe wall for different levels of internal corrosion and cross-sectional reduction.

5 | Conclusion

In the present study, the hydrodynamic effects of internal corrosion and rust buildup in water transmission pipelines were investigated using computational fluid dynamics analysis. Several cases of corrosion with different geometries were investigated to examine their effects on streamlines, velocity profiles, vortex generation, and pressure coefficients.

From the numerical simulation, it was noted that as the corrosion intensity increases, the flow inside the pipeline changes. In the smooth pipe, the flow is relatively steady and symmetric, with uniform streamline patterns. However, as corrosion intensity increases, the effective flow area decreases, leading to fluid acceleration. In addition, higher velocity and an adverse pressure gradient were observed due to corrosion within the pipe.

In this study, it was also shown that under high-corrosion conditions, significant separation and vortical flow occur at the back end of the contraction zone. Vortical flow increases turbulence within the pipe, thereby causing losses. Furthermore, the pressure coefficient distribution showed an increase in pressure coefficient as corrosion intensity increased. The pressure coefficient was maximized for the highly corroded condition. Confronting the numerical analysis results with those obtained experimentally for the sudden expansion flow revealed that the RNG $k-\varepsilon$ turbulence model provides satisfactory predictions of separated turbulent flow and the regions of recirculation. Generally, it can be concluded that internal corrosion not only reduces the efficiency of water supply through pipelines but also increases energy losses associated with higher pressures.

Further research might include analysis of the influence of transient flow regime, 3D geometries of the corrosion, multiphase behavior, and experimentally based analysis of turbulence under the influence of corrosion.

Conflict of Interest

The authors declare that there is no conflict of interest regarding the publication of this article.

Data Availability

All data generated or analyzed during this study are included in this published article. No additional data are available.

Funding

This research did not receive any specific grant from funding agencies in the public, commercial, or not-for-profit sectors.

References

[1] Perry, A. E., Schofield, W. H., & Joubert, P. N. (1969). Rough wall turbulent boundary layers. *Journal of fluid mechanics*, *37*(2), 383–413. https://doi.org/10.1017/S0022112069000619

[2] Silberman, E. (1970). Effect of helix angle on flow in corrugated pipes. *Journal of the hydraulics division*, *96*(11), 2253–2263. https://doi.org/10.1061/JYCEAJ.0002760

[3] Silberman, E. (1980). Turbulence in helically corrugated pipe flow. *Journal of the engineering mechanics division*, *106*(4), 699–717. https://doi.org/10.1061/JMCEA3.0002619

[4] Chen, J. J. J., Leung, Y. C., & Ko, N. W. M. (1986). Drag reduction in a longitudinally grooved flow channel. *Industrial & engineering chemistry fundamentals*, *25*(4), 741–745. https://doi.org/10.1021/i100024a044

[5] Djenidi, L., Antonia, R. A., & Anselmet, F. (1994). LDA measurements in a turbulent boundary layer over a d-type rough wall. *Experiments in fluids*, *16*(5), 323–329. https://doi.org/10.1007/BF00195431

[6] Morales, R. E. M., Franco, A. T., Junqueira, S. L. M., & Erthal, R. H. (2007). *Experimental analysis of turbulent flow in flexible pipes*.

[7] Hu, H., & Cheng, Y. F. (2016). Modeling by computational fluid dynamics simulation of pipeline corrosion in CO2-containing oil-water two phase flow. *Journal of petroleum science and engineering*, *146*, 134–141. https://doi.org/10.1016/j.petrol.2016.04.030

[8] Li, Q., Hu, H., & Cheng, Y. F. (2016). Corrosion of pipelines in CO2-saturated oil-water emulsion flow studied by electrochemical measurements and computational fluid dynamics modeling. *Journal of petroleum science and engineering*, *147*, 408–415. https://doi.org/10.1016/j.petrol.2016.09.011

[9] Pouraria, H., Seo, J. K., & Paik, J. K. (2016). A numerical study on water wetting associated with the internal corrosion of oil pipelines. *Ocean engineering*, *122*, 105–117. https://doi.org/10.1016/j.oceaneng.2016.06.022

[10] Kahyarian, A., Singer, M., & Nesic, S. (2016). Modeling of uniform CO2 corrosion of mild steel in gas transportation systems: A review. *Journal of natural gas science and engineering*, *29*, 530–549. https://doi.org/10.1016/j.jngse.2015.12.052

[11] Owen, J., Godfrey, J., Ma, W., de Boer, G., Al-Khateeb, M., Thompson, H., … & Barker, R. (2020). An experimental and numerical investigation of CO2 corrosion in a rapid expansion pipe geometry. *Corrosion science*, *165*, 108362. https://doi.org/10.1016/j.corsci.2019.108362

[12] Wang, W., Sun, Y., Wang, B., Dong, M., & Chen, Y. (2022). CFD-Based Erosion and Corrosion Modeling of a Pipeline with CO2-Containing Gas–Water Two-Phase Flow. *Energies*, *15*(5), 1694. https://doi.org/10.3390/en15051694

[13] Zeng, L., Lv, T., Chen, H., Ma, T., Fang, Z., & Shi, J. (2023). Flow accelerated corrosion of X65 steel gradual contraction pipe in high CO2 partial pressure environments. *Arabian journal of chemistry*, *16*(8), 104935. 10.1016/j.arabjc.2023.104935

[14] Thorat, U., Jones, M., Woollam, R., Owen, J., Barker, R., Thompson, H., & de Boer, G. (2024). Computational fluid dynamics driven mass transfer model for the prediction of CO2 corrosion in pipelines. *Journal of pipeline science and engineering*, *4*(1), 100148. https://doi.org/10.1016/j.jpse.2023.100148

[15] Yang, H., Lu, L., Tsai, K., & Sidahmed, M. (2023). A hybrid physics and active learning model for cfd-based pipeline co2 and o2 corrosion prediction. *International petroleum technology conference* (p. D031S037R003). IPTC. https://doi.org/10.2523/IPTC-23049-EA

[16] Cruz, D., Anbarlooei, H., Ramos, F., Santos, C., & Celis, G. (2023). On the attached eddy hypothesis and the turbulent friction factor of pipe flows with rough wall. *Bulletin of the american physical society*. https://meetings.aps.org/Meeting/DFD23/Session/G42.5

[17] Wang, H., Li, Z., Zhang, Z., Wang, Y., Xu, Z., Fan, P., … & Yu, Q. (2023). The Relationship between the Flow Velocity of Freshwater and the Corrosion Performance of Steel Pipe Elbow Sections in Water Resource Allocation Engineering. *Journal of materials engineering and performance*, *32*(11), 4941–4958. https://doi.org/10.1007/s11665-022-07432-w

[18] Obaseki, M., Alfred, P. B., Elijah, P. T., & Okuma, S. O. (2023). Corrosion rate prediction in oil and gas pipelines based on multiphase flow modelling. *International journal of engineering research in africa*, *67*, 27–48. https://doi.org/10.4028/p-brqaI1

[19] Thangam, S., & Speziale, C. G. (1992). Turbulent flow past a backward-facing step-A critical evaluation of two-equation models. *AIAA journal*, *30*(5), 1314–1320. https://ui.adsabs.harvard.edu/link_gateway/1992AIAAJ..30.1314T/doi:10.2514/3.11066